# Retraction criteria of viscoplastic drops and sheets : long-wave approximations

Hiranya Deka, Jean-Lou Pierson, Edson J. Soares

# Retraction criteria of viscoplastic drops and sheets: long-wave approximations

Hiranya Deka[a,*], Jean-Lou Pierson[a], Edson J. Soares[a,b]

[a] *IFP Energies nouvelles, Rond-point de l'échangeur de Solaize, 69360 Solaize, France*
[b] *LABREO, Department of Mechanical Engineering, Universidade Federal do Espirito Santo, Avenida Fernando Ferrari, 514, Goiabeiras, 29075-910, ES, Brazil*

**Abstract**

Retraction dynamics of viscous drops and sheets depend on the relative magnitude of the viscous force over the capillary force. The dynamics are more complicated in the case of viscoplastic drops/sheets because the yield stress of the fluid also comes into play. The retraction of slender viscoplastic drops and sheets depends on the relative magnitude of the yield stress over the capillary stress. Depending on its relative magnitude, the yield stress can completely resist the retraction. In this study, the retraction of viscoplastic drops and sheets has been investigated theoretically neglecting the effect of the surrounding medium. Using long-wave theory we derive the retraction criteria of slender drops (axisymmetric) and sheets (two-dimensional) for yield stress fluids. Direct numerical simulations are also performed by solving the complete momentum conservation equations. A good agreement is found between the numerical results and the proposed retraction criteria.
*Keywords:* Viscoplastic fluid, Capillary flow, Long-wave theory, Retraction

*Corresponding Author
*Email addresses:* hiranya.deka@ifpen.fr; hiranyadeka.mech@gmail.com (Hiranya Deka ), +33437703216 (Hiranya Deka )

## 1. Introduction

Retraction of Newtonian liquid drops or sheets is a classical problem in fluid mechanics which has been studied by many researchers over two centuries. Based on observations of soap film rupture, Dupré [1] derived a velocity for the retracting rim using energy balance. Later on, using momentum balance Taylor [2] and Culick [3] individually showed that the retraction velocity is $\sqrt{2}$ times less than that predicted by Dupré's formula. Their theoretical prediction was confirmed experimentally by McEntee & Mysels [4] for sheets of thickness larger than 1 $\mu$m.

In the case of a Newtonian fluid, two dimensionless parameters govern the problem. The initial aspect ratio of the drop/sheet and the Ohnersorge number ($Oh = \mu/\sqrt{\rho\sigma R_0}$) which is the ratio of the viscous-capillary time scale $t_v = \mu R_0/\sigma$ and the inertia-capillary time scale $t_c = (\rho R_0^3/\sigma)^{1/2}$ where $\mu$ is the viscosity of the liquid, $\rho$ is the density of the liquid, $\sigma$ is the surface tension coefficient and $R_0$ is the initial radius of the slender drop (in the case of a liquid sheet it is half of the initial thickness, $h_0$). In the low $Oh$ number limit, the flow is governed by a balance between inertia and capillary force and, the drops/sheets retract at Taylor-Culick velocity with the formation of a bulbous end. On the other hand, in the high Ohnesorge number limit the retraction is mainly resisted by the viscous force and the drops/sheets retract with a uniform increase in radius/thickness [5, 6]. However, inertia might become important even in the large $Oh$ limit for very long drops/sheets [7, 8].

The fundamental dynamics of retraction is significantly affected in the

case of viscoplastic fluids. The viscoplastic fluids exhibit the characteristics of a solid if the applied/induced stress is below a critical value (called yield stress) and behaves like a fluid above the yield stress limit. One needs to consider one more dimensionless parameter (compared with a Newtonian fluid) to take into account the yield stress of the material. This parameter has a dramatic influence on the retraction dynamics of the drops/sheets for moderate and high Ohnesorge numbers [9]. Indeed, the retraction of the drops/sheets can be completely resisted by the yield stress of the viscoplastic material. Therefore the natural question that arises here is what are the criteria of retraction for slender drops and sheets in the case of a yield stress fluid.

The stopping/flowing criteria of viscoplastic fluids for different geometric configurations have received the attention of several researchers. For example, the critical pressure gradient in the Poiseuille flow of viscoplastic fluids is studied in Refs. [10] & [11]. The critical limit for the motion of a solid sphere in a viscoplastic fluid is studied in Ref. [12] while the yield limit for the motion of a bubble in a yield stress fluid is studied in Refs. [13] & [14]. Here, we report the critical limits for the retraction of slender drops and sheets of yield stress fluids.

In order to answer this problem, we use a combination of direct numerical simulations and long-wave models of drops and sheets. The long-wave models are convenient tools to study the retraction of slender sheets and drops. Earlier, several researchers have used this theory to study drop/sheet retraction for the Newtonian fluid [5, 6, 15]. However, there are very limited studies for the yield stress fluids. The long-wave model equations for the

yield stress fluids were first developed by Balmforth et al. [16] for an axisymmetric configuration to study the Rayleigh instability and the pinch-off of a cylindrical jet in extensional flow. Here, we have used those long-wave equations to study the retraction of slender drops. We also present the long-wave model equations in the two-dimensional coordinate system to study the retraction of slender liquid sheets. Direct numerical simulations are also performed by solving the complete momentum conservation equations to study the retraction of drops and sheets. An open-source volume-of-fluid method based two-phase flow solver called *Basilisk* [17, 18, 19, 20] is used to perform the numerical simulations. The retraction dynamics of a two-dimensional viscoplastic sheet has already been discussed Ref. [9]. We have observed similar retraction dynamics for axisymmetric drops, which are not repeated here. Here, we are interested only in the boundary between the retraction and no-retraction regimes. Numerical simulations corroborate that the retraction criteria derived here using the long-wave model are more accurate that the criterion presented in Ref. [9] using simple scaling arguments. The rest of the paper is arranged as follows: first, we present an analysis to find the retraction criteria using the long-wave theory for axisymmetric drops and two-dimensional sheets. Next, we compare the theoretical analysis with the direct numerical simulations. Finally, we wind up with a discussion and concluding remarks.

## 2. Retraction criteria based on long-wave model

Here, we derive the retraction criteria for the axisymmetric drops and two-dimensional sheets using the long-wave theory. We neglect the effect of the surrounding medium. The rheology of the viscoplastic material is

modeled using the Bingham model [21] where the constitutive relation for the deviatoric stress tensor $\boldsymbol{\tau}$ is given as

$$\begin{cases} \boldsymbol{\tau} = \left(\mu_p + \frac{\tau_y}{\dot{\gamma}}\right)\dot{\boldsymbol{\gamma}}, & \text{if} \quad \tau > \tau_y \quad \text{and} \\ \dot{\boldsymbol{\gamma}} = 0, & \text{otherwise.} \end{cases} \tag{1}$$

Here, $\dot{\boldsymbol{\gamma}}$ is the strain-rate tensor; $\mu_p$ is the plastic viscosity of the viscoplastic material; $\tau_y$ is the yield stress of the viscoplastic material; $\tau = \sqrt{(1/2)\boldsymbol{\tau} : \boldsymbol{\tau}}$ and $\dot{\gamma} = \sqrt{(1/2)\boldsymbol{\gamma} : \boldsymbol{\gamma}}$ are the second invariants.

Using the initial drop radius $R_0$ ($h_0$ for sheets) as the characteristic length scale and inertia-capillary time $t_c = \sqrt{\rho R_0^3/\sigma}$ ($t_c = \sqrt{\rho h_0^3/\sigma}$ for sheets) as the characteristic time scale, we find that two dimensionless parameters govern the problem of interest: the Ohnesorge number ($Oh = \mu_c/\sqrt{\rho\sigma R_0}$) and the plastic number ($Pl = \tau_y/(\mu_c\dot{\gamma}_c)$) which represents the plastic nature (related to yield stress) of the fluid [22, 9]. Here, $\dot{\gamma}_c$ is the characteristic strain rate and is estimated as $\dot{\gamma}_c = 1/t_c$, and, $\mu_c = \mu_p + \tau_y/\dot{\gamma}_c$ is the characteristic viscosity (see Ref. [9] for more details). We determine the retraction criteria in terms of these dimensionless parameters. By choosing the initial drop radius $R_0$ ($h_0$ for sheets) as the characteristic length scales in both radial and axial direction, we have implicitly assumed that the initial aspect ratio of the drop does not play a significant role in the retraction process. This assumption will be discussed at the end of Sec. 3.

### *2.1. Axisymmetric drop*

The representative diagram of the geometry is shown in Fig. 1. We consider a cylindrical coordinate system $(r, z)$ to model the flow where the axis of symmetry lies in the $z$-direction. The major axis of the slender drop is

aligned to the axis of symmetry. For a slender drop of radius $R$, the long-wave equations are given as [16]

$$\frac{\partial R^2}{\partial t} + \frac{\partial \left(u_z R^2\right)}{\partial z} = 0, \tag{2}$$

$$\frac{\partial u_z}{\partial t} + u_z \frac{\partial u_z}{\partial z} = -\frac{2\sigma}{\rho}\frac{\partial \kappa}{\partial z} + \frac{3}{2}\frac{1}{\rho R^2}\frac{\partial}{\partial z}\left(R^2 \tau_{zz}\right). \tag{3}$$

Here, $u_z$ is the axial velocity inside the drop and $\kappa$ corresponds to the mean curvature given as

$$\kappa = \frac{1}{2}\left(\frac{1/R}{\left(1+(\partial R/\partial z)^2\right)^{1/2}} - \frac{\partial^2 R/\partial z^2}{\left(1+(\partial R/\partial z)^2\right)^{3/2}}\right), \tag{4}$$

and $\tau_{zz}$ is the deviatoric stress tensor component. These leading-order equations are derived on the asymptotic limit $R_0/L_0 = \epsilon \ll 1$ i.e. the characteristic radius of the slender drop $R_0$ is much smaller than the axial length scale $L_0$. Such an assumption leads to a derivative imbalance $\partial/\partial z \sim \epsilon \partial/\partial r$. Inserting those scalings in the mass conservation equation implies that the radial velocity is much smaller than the axial velocity. Those estimates are used in deriving the long-wave model equations. However, the scaling for the shear rate requires more care since to leading order the longitudinal velocity is independent of the radial coordinate [23]. Hence the shear rate scales as $\epsilon^2 U_z/R_0$, where $U_z$ is the axial velocity scale. Due to this scaling, the shear stress is $O(\epsilon)$ smaller than the normal stresses; see Ref. [16] for a more elaborate discussion. By using the normal and tangential stress balance at the column interface, the long-wave equations can be obtained. They are similar to the case of Newtonian fluids; the only difference appears via the Bingham constitutive relation given in Eq. (1). The long-wave scaling reduces the

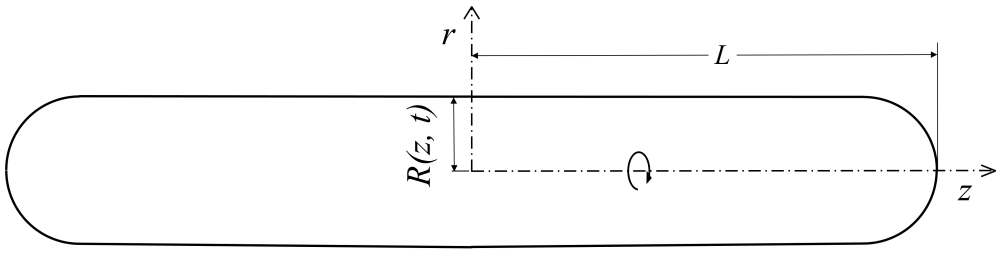


Figure 1. A representative diagram of the geometry of a slender drop.

Bingham constitutive relation to

$$\begin{cases} \tau_{zz} = 2\left(\mu_p + \frac{\tau_y}{\sqrt{3}|\partial u_z/\partial z|}\right)\frac{\partial u_z}{\partial z} & \text{if} \quad \frac{\sqrt{3}|\tau_{zz}|}{2} > \tau_y \quad \text{and} \\ \frac{\partial u_z}{\partial z} = 0 \quad \text{otherwise,} \end{cases} \tag{5}$$

where the yield criterion is

$$\frac{\sqrt{3}|\tau_{zz}|}{2} > \tau_y. \tag{6}$$

Now, we use those equations to find the retraction criterion of a slender viscoplastic drop. We assume that the Ohnesorge number is sufficiently large such that the retraction process is resisted by viscous effect only [7]. Therefore, considering the flow as Stokes flow and hence neglecting the inertial terms, Eq. (3) can be written as

$$0 = -\frac{2\sigma}{\rho}\frac{\partial \kappa}{\partial z} + \frac{3}{2}\frac{1}{\rho R^2}\frac{\partial}{\partial z}\left(R^2\tau_{zz}\right). \tag{7}$$

Using Eq. (4) for the mean curvature, Eq. (7) can be rewritten as

$$\frac{2\sigma}{3}\frac{\partial}{\partial z}\left[\frac{R}{\left(1+(\partial R/\partial z)^2\right)^{1/2}} + \frac{R^2\partial^2 R/\partial z^2}{\left(1+(\partial R/\partial z)^2\right)^{3/2}}\right] + \frac{\partial}{\partial z}\left(R^2\tau_{zz}\right) = 0. \tag{8}$$

Now we integrate the above equation from a point away from the tip (written as $z$) to the tip of the drop ($z = L_0$). The slender drop is assumed to be cylindrical with hemispherical ends. Therefore, we have the following boundary conditions to evaluate the integral: at the end of the drop i.e. at $z = L_0, R = 0, \partial R/\partial z = \infty$. At any other location ($z$) away from the tip of the drop we have $R = R_0$, $\partial R/\partial z = 0$ and $\partial^2 R/\partial z^2 = 0$. Applying these boundary conditions to evaluate the integral leads to the following simplified equation

$$\frac{2}{3}\sigma R_0 + R_0^2 \tau_{zz} = 0. \tag{9}$$

Now, using the value of $\tau_{zz}$ from Eq. (9) in the yielding criterion given in Eq. (6) we get

$$\begin{aligned} \frac{\sqrt{3}|\tau_{zz}|}{2} = \frac{\sqrt{3}}{2}\frac{2\sigma}{3R_0} > \tau_y \\ \text{or} \quad \frac{\tau_y R_0}{\sigma} < \frac{1}{\sqrt{3}} \end{aligned} \tag{10}$$

In terms of the dimensionless parameters it can be represented as

$$Oh \times Pl < \frac{1}{\sqrt{3}} \tag{11}$$

Equation (11) gives the retraction criterion of a slender viscoplastic drop in terms of the dimensionless parameters considered here. The quantity $\tau_y R_0/\sigma (\equiv Oh \times Pl)$ is also called Bingham-capillary number [24, 25] which represents the relative magnitude of the yield stress over the capillary stress.

### *2.2. Two-dimensional sheet*

A representative diagram of the geometry is shown in Fig. 2. We consider a two-dimensional Cartesian coordinate system $(x, y)$ where the slender sheet

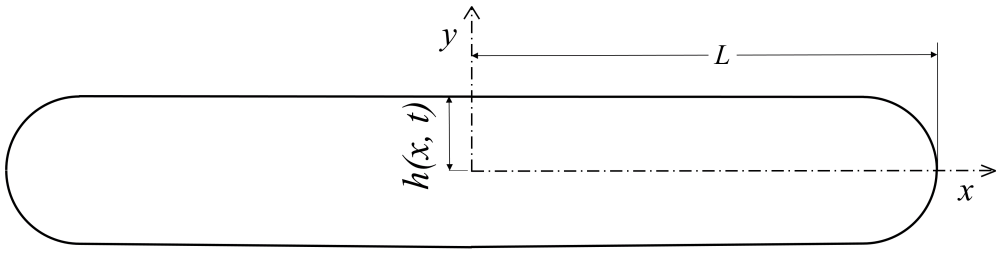


Figure 2. A representative diagram of the geometry of a two-dimensional slender liquid sheet.

is aligned to the $x-$axis. We present the long-wave equation for a slender two-dimensional sheet in the asymptotic limit $h_0/L_0 \ll 1$, where $h_0$ and $L_0$ are the characteristic length scales along ($x$-direction) and perpendicular ($y$-direction) to the slender sheet respectively. We follow the same procedure and scaling as proposed by Erneux & Davis [26], but we explicitly keep the non-negligible part of the viscous stress tensor as done by Balmforth et al. [16] while deriving the long-wave equations for a slender drop. The viscoplastic long-wave equations in a two-dimensional coordinate system can be written as

$$\frac{\partial h}{\partial t} + \frac{\partial}{\partial x}\left(hu\right) = 0 \tag{12}$$

and

$$\frac{\partial u}{\partial t} + u\frac{\partial u}{\partial x} = -\frac{\sigma}{\rho}\frac{\partial \kappa}{\partial x} + \frac{2}{\rho h}\frac{\partial}{\partial x}\left(\tau_{xx} h\right). \tag{13}$$

Here, $h(x,t)$ is half of the sheet thickness, $u$ is the velocity along the $x-$axis, $\kappa$ is the curvature which can be written as

$$\kappa = -\frac{\partial^2 h/\partial x^2}{\left(1 + \left(\partial h/\partial x\right)^2\right)^{3/2}}, \tag{14}$$

and $\tau_{xx}$ is the deviatoric stress tensor component. The Bingham constitutive relation (1) under such a condition reduces to

$$\begin{cases} \tau_{xx} = 2\left(\mu_p + \frac{\tau_y}{2|\partial u/\partial x|}\right)\frac{\partial u}{\partial x} & \text{if } |\tau_{xx}| > \tau_y, \\ \frac{\partial u}{\partial x} = 0 & \text{otherwise,} \end{cases} \tag{15}$$

where the yielding criterion is

$$|\tau_{xx}| > \tau_y. \tag{16}$$

Similar to the previous section, we aim to find the criterion of retraction for a slender sheet. Therefore, following the same assumptions mentioned in the previous section and replacing the curvature $\kappa$ using Eq. (14), we rewrite Eq. (13) as

$$2\frac{\partial}{\partial x}\left(\tau_{xx}h\right) - \sigma\frac{\partial}{\partial x}\left(-\frac{h\left(\partial^2 h/\partial x^2\right)}{\left(1+\left(\partial h/\partial x\right)^2\right)^{3/2}} - \frac{1}{\left(1+\partial h/\partial x\right)^{1/2}}\right) = 0. \tag{17}$$

Now, we integrate Eq. (17) from any location away from the tip ($x$) to the tip of the liquid sheet ($x = L_0$). To evaluate the integral we have similar boundary conditions as that of an axisymmetric drop: at end-tip of the liquid sheet i.e. at $x = L_0$, we have $h = 0, \partial h/\partial x = \infty$. At any location away from the tip, the liquid sheet is assumed to be flat and we have $h = h_0, \partial h/\partial x = 0$ and $\partial^2 h/\partial x^2 = 0$. The integration of Eq. (17) with the above boundary conditions leads to the following simplified equation

$$2\tau_{xx}h_0 + \sigma = 0. \tag{18}$$

Using the value of $\tau_{xx}$ from Eq. (18) in the yielding criterion (16) we have

$$\tau = |\tau_{xx}| = \frac{\sigma}{2h_0} > \tau_y \quad \text{or} \quad \frac{\tau_y h_0}{\sigma} < \frac{1}{2}. \tag{19}$$

In terms of the dimensionless parameters it can be represented as

$$Oh \times Pl < \frac{1}{2}. \tag{20}$$

Therefore, in the case of a two-dimensional sheet, the product $Oh \times Pl$ should be less than $1/2$ for the start of retraction. According to the long-wave theory, the critical limit is lower in this case compared with an axisymmetric drop where the critical limit is found to be $1/\sqrt{3}$.

## 3. Numerical simulations

In order to validate the theory, we have performed direct numerical simulations using the Basilisk solver. The numerical simulations are performed using a regularized version of the model [27]. The complete detail of the numerical methodology is available in Ref. [9]. The range of the dimensionless parameters considered in the simulations are: $Oh = 0.1 - 10$, $Pl = 0.1 - 0.9$ and except at the end of the present section, all the simulations are initialized with a constant aspect ratio $L_0/R_0$ (or $L_0/h_0$) $= 10$. The simulations are performed with a Newtonian surrounding fluid having density ratio (density of the surrounding medium divided by the density of the viscoplastic material) of 0.001 and viscosity ratio (viscosity of the surrounding medium divided by the viscosity of the viscoplastic material) lesser than 0.001 (maximum viscosity ratio when the value of $\tau_y$ is zero; see Ref. [9] for more details).

To determine the retraction of the drops/sheets we plot the yielded and the unyielded regions within the drop/sheet at different time instants. If the drop/sheet undergoes retraction we see yielded regions within it. On the other hand, if there is no yielded region within the drop/sheet, we affirm that the drop/sheet does not undergo retraction. This is a better criterion to

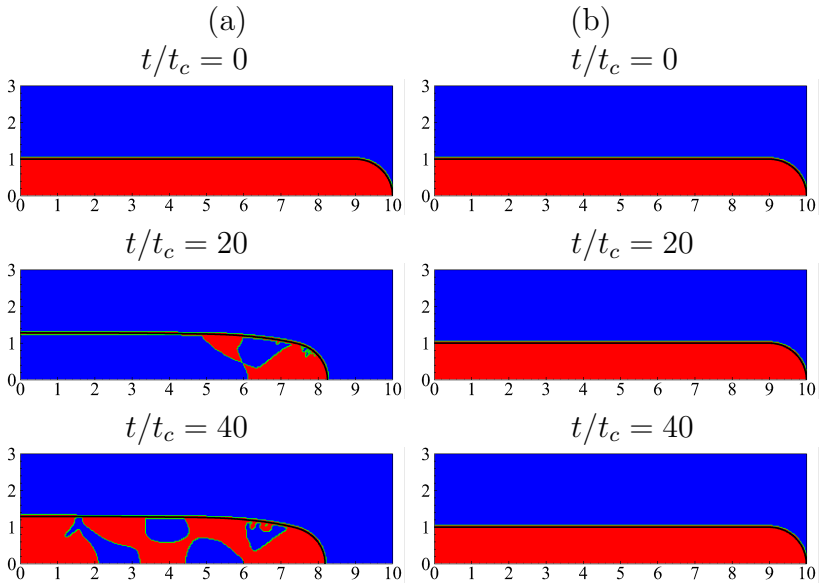


Figure 3. The yielded (blue) and unyielded (red) regions within the viscoplastic liquid sheet for $Oh = 2.0$ and two different values of plastic number: (a) $Pl = 0.2$ and (b) $Pl = 0.3$. The plots are shown at a dimensionless time interval of $\Delta t/t_c = 20$. The interface profile at different time instants is shown by the black line.

separate the retracting and non-retracting regimes than the velocity based criteria used in Ref. [9]. This is because we have used a regularized Bingham model to perform the numerical simulations where the infinite viscosity of the Bingham material is replaced by a high viscosity. Although we have rigorously tested this parameter before fixing its value such that the numerical results do not depend on this parameter (see Ref. [9]), still the regularized model gives rise to a small velocity in each grid cell even in the unyielded state. It is difficult to separate out whether the velocity is induced due to the regularized model or due to the actual retraction of the drop/sheet at the limiting condition because the drop/sheet retracts very slowly near the critical limit. Because of that, small uncertainties in the results were observed in Ref. [9] near the critical limit. The plotting of the yielded/unyielded regions

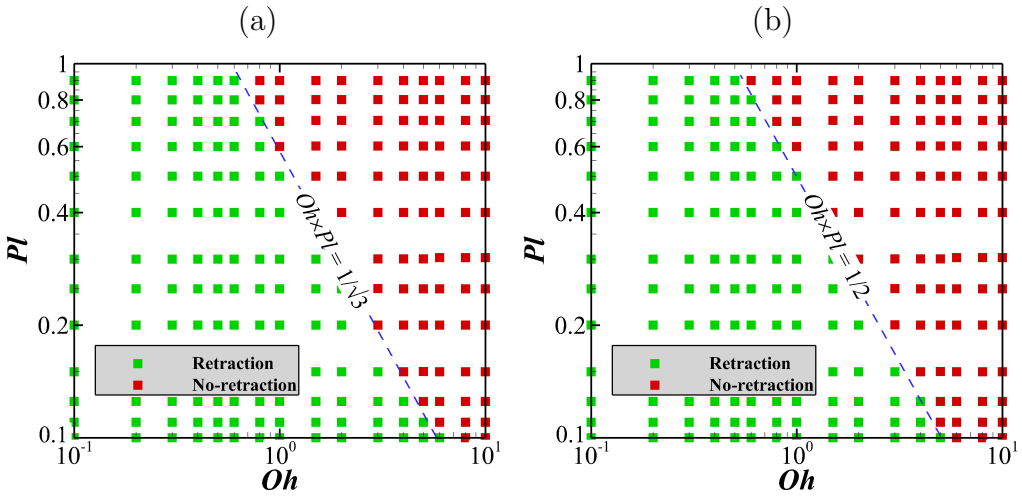


Figure 4. A regime map showing the retraction and no-retraction points in the $Oh - Pl$ plane for (a) axisymmetric drops and (b) two-dimensional sheets. The red squares represent the points where the drop retraction is resisted by the yield stress of the viscoplastic material and the green squares represent the points where the viscoplastic drops/sheets retract overcoming the yield stress of the material. Initial aspect ratio is 10 in all the numerical simulations considered here.

improves the accuracy and the interpretation of the numerical results.

Bingham model suggests that the material undergoes yield when the second invariant of the deviatoric stress tensor exceeds the yield stress of the material. Few sample plots of the yielded/unyielded regions at different time instants for $Oh = 2$ and two different plastic numbers: (a) $Pl = 0.2$ and (b) $Pl = 0.3$ are shown in Fig. 3. In Fig. 3 (a) the capillary force is able to overcome the yield stress of the material which results in the yielding of the material and retraction of the sheet. On the other hand, it is evident in Fig. 3 (b) that the sheet remains completely unyielded. Here, the capillary stress is not able to overcome the yield stress of the material and the liquid sheet does not undergo retraction.

The data obtained from numerical simulations are presented in Fig. 4 in the $Oh - Pl$ maps. Figure 4 (a) shows the numerical results for axisymmetric

drops while Fig. 4 (b) shows the data for the two-dimensional liquid sheets. For each configuration, we have performed approximately 250 simulations. The green squares represent the points where the drop/sheet undergoes retraction and the red squares represent the points where the retraction of the drop/sheet is resisted by the yield stress of the viscoplastic material. A very good match is obtained between the numerical results and the theoretical predictions (Eqs. (11) and (20)) for both geometries. Even though the retraction criteria are developed under the assumption of negligible inertia effect or large $Oh$, it is evident that these criteria work well even for small $Oh$, for example, $Oh$ as small as 0.5 in the case of two-dimensional sheets. For this $Oh$ value, the retraction criterion gives $Pl \approx 1$. The yield stress is thus sufficiently large to resist the appearance of momentum in the slender sheet (or drop) at the start of retraction and as a consequence, the inertia remains negligible.

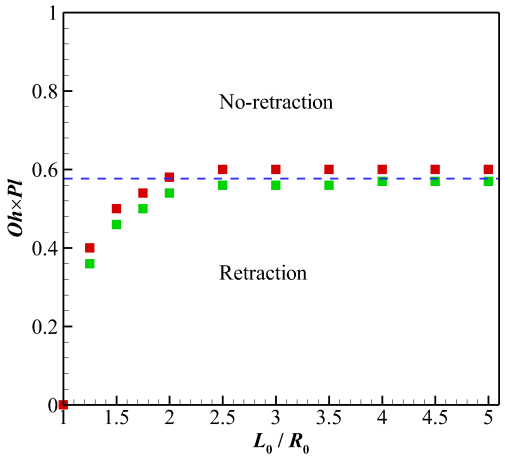


Figure 5. Numerical results showing the retraction and no-retraction regimes of an axisymmetric drop as a function of the initial aspect ratio $L_0/R_0$. The red squares represent the points where the drop retraction is resisted by the yield stress and the green squares represent the points where the viscoplastic drops undergo retraction. The dotted line is the theoretical prediction (11).

The retraction starts when the capillary pressure difference near the tip region exceeds the yield stress which is independent of the initial aspect ratio. However, the long-wave models are derived under the assumption of slender shape. Therefore, it is important to check the validity of the proposed model as a function of the initial aspect ratio. We run a series of simulations by sequentially increasing the aspect ratio from 1 to 10. The numerical results showing the critical bound for two different values of $Oh$ (1.0 and 2.0) are presented in Fig. 5. The results are in good agreement with the theoretical prediction for $L_0/R_0 \geq 2.5$. This lower bound is because of the aforementioned limitations of the long-wave models, i.e. $L_0/R_0 \gg 1$, which are not valid anymore for small aspect ratios. For aspect ratio smaller than 2.5, the critical limit decreases gradually (later sharply) as the aspect ratio decreases. The retraction is resisted by a lower value of plasticity at small aspect ratios as compared with large aspect ratios. In other words, retraction is more difficult at a small aspect ratio. Finally, since the spherical shape is an equilibrium position for the drop, there is no motion for $L_0/R_0 = 1$ irrespective of the value of $Oh \times Pl$.

## 4. Discussion and concluding remarks

In Sec. 2 we have derived the criteria (Eqs. (10) and (19)) for the start of retraction. However, it has been observed in the numerical simulations that in many cases the retraction starts and undergoes for some initial period, and then it stops. In other words, the difference of capillary pressure overcomes the yield stress at the start initiating the retraction. However, after an initial period, the capillary stress is not able to overcome the yield stress of the material and the plastic nature of the material resumes. The analysis of

Sec. 2 can be straightforwardly generalized to this configuration where the retraction starts and then it stops. The boundary conditions and assumptions are similar to those mentioned in Sec. 2.1 and 2.2 except that we perform the integration at any arbitrary time instant $t$ when the drop radius is $R$ (or half-sheet thickness is $h$) and half-length is $L$ which were $R_0$ (or $h_0$) and $L_0$ at $t = 0$. After integration and some algebra, we get similar criteria for retraction but in a general form valid at any time instant $t$

$$\begin{cases} \frac{\tau_y R}{\sigma} < \frac{1}{\sqrt{3}} & \text{for drops,} \\ \frac{\tau_y h}{\sigma} < \frac{1}{2} & \text{for sheets,} \end{cases} \tag{21}$$

or, in terms of the dimensionless numbers

$$\begin{cases} (Oh \times Pl) \times \left(\frac{R}{R_0}\right) < \frac{1}{\sqrt{3}} & \text{for drops,} \\ (Oh \times Pl) \times \left(\frac{h}{h_0}\right) < \frac{1}{2} & \text{for sheets.} \end{cases} \tag{22}$$

At the start of retraction $R = R_0$ and $h = h_0$, and therefore the criteria are given by Eqs. (11) and (20). The liquid drop/sheet retracts initially when this condition is satisfied. The drop radius $R$ (or sheet thickness $h$) increases with time as the drop (or sheet) retracts, and at some instant, the quantity $(Oh \times Pl)R/R_0$ (or $(Oh \times Pl)h/h_0$) becomes larger than $1/\sqrt{3}$ (or $1/2$) and does not satisfy the criteria given in Eq. (22) to continue the retraction .

Figure 6 shows the interface profiles and yielded/unyielded regions within a drop at different instants of time for two different configuration of dimensionless parameters. It is evident in Fig. 6 (a) and (b) that the drop retracts for a initial period (see at $t/t_c = 10$) and stops later. The dimensionless parameters considered in Fig. 6 (a) and (b) are $Oh = 2.0, Pl = 0.25$ and

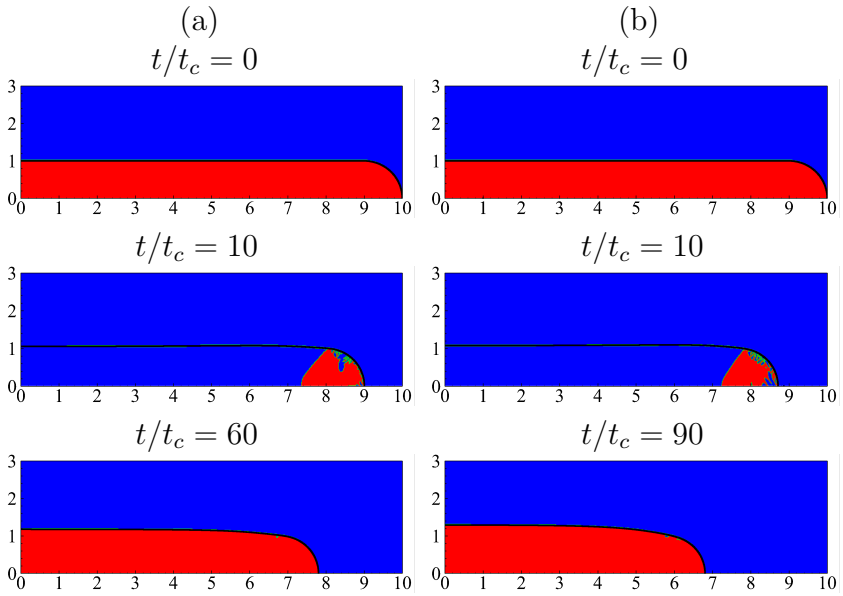


Figure 6. The yielded (blue) and unyielded (red) regions within the viscoplastic slender drops for (a) $Oh = 2.0$, $Pl = 0.25$ and (b) $Oh = 3.0$, $Pl = 0.15$ at different time instants. The interface profile at each time instant is shown by the black line.

$Oh = 3.0, Pl = 0.15$, which should undergo retraction according to Eq. (11). As the drop undergoes retraction, the drop radius increases in a uniform way because of higher $Oh$ [8]. The prediction of Eq. (22) suggests that the retraction should stop as the value $R/R_0$ exceeds 1.155 in (a) and 1.283 in (b) which is evident in Fig. 6 (a) and (b) at $t/t_c = 60$ and $t/t_c = 90$, respectively. The radius of the drop is found to be approximately 1.172 in (a) and 1.288 in (b) in the final rigid states which are in good agreement with the aforementioned criteria.

The next question that comes in mind is how inertia contributes to the final rigid shape of the drop/sheet. To get a qualitative idea of the inertia effect on the final shape we plot the ratio of the final radius of the drop to its

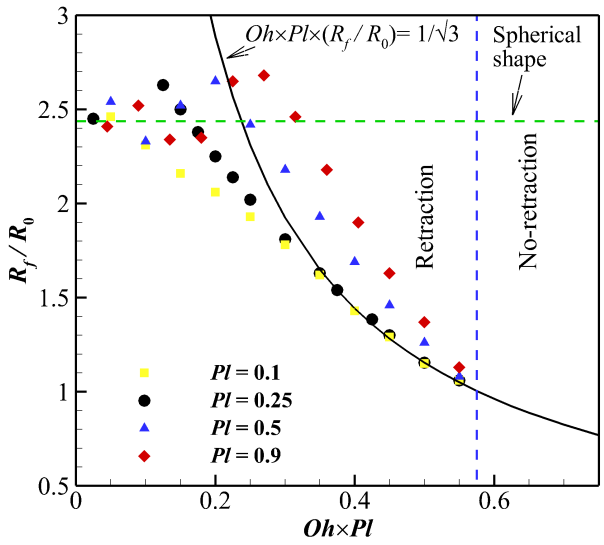


Figure 7. The ratio between the radius of the drop in the final rigid state and its initial radius ($R_f/R_0$) is plotted as a function of $Oh \times Pl$. The axisymmetric simulations are performed for four values of $Pl$ (0.1, 0.25, 0.5, and 0.9), and for each $Pl$ the value of $Oh \times Pl$ is changed by changing the $Oh$. The black line shows the theoretical prediction (22) for an axisymmetric drop. The blue dashed line is the retraction criterion (11). The initial aspect ratio in all the simulations is 10 and the green dashed line represents the final radius of a sphere having same volume as that of the slender drops.

initial radius ($R_f/R_0$) as a function of $Oh \times Pl$ for fixed values of $Pl$ and by sequentially increasing the inertial effect (decreasing the $Oh$). Such a plot is presented in Fig. 7 which shows the comparison of the numerical data with the prediction of Eq. (22) (shown by the black solid line) for four different values of $Pl$, viz. $Pl = 0.1$, 0.25, 0.5, and 0.9. According to Eq. (11), the critical $Oh$ value for undergoing retraction decreases as the plasticity increases. The maximum limit of $Oh$ is approximately 5.77, 2.31, 1.14 and 0.64 for the corresponding $Pl$ values 0.1, 0.25, 0.5 and 0.9 respectively. It is evident in Fig 7 that for $Pl = 0.1$ and 0.25, the agreement between the theoretical prediction and the numerical results is good for $Oh \times Pl > 0.3$; the deviation increases below this value. For $Pl = 0.5$, a noticeable deviation is observed from the theoretical criterion. This is because the corresponding

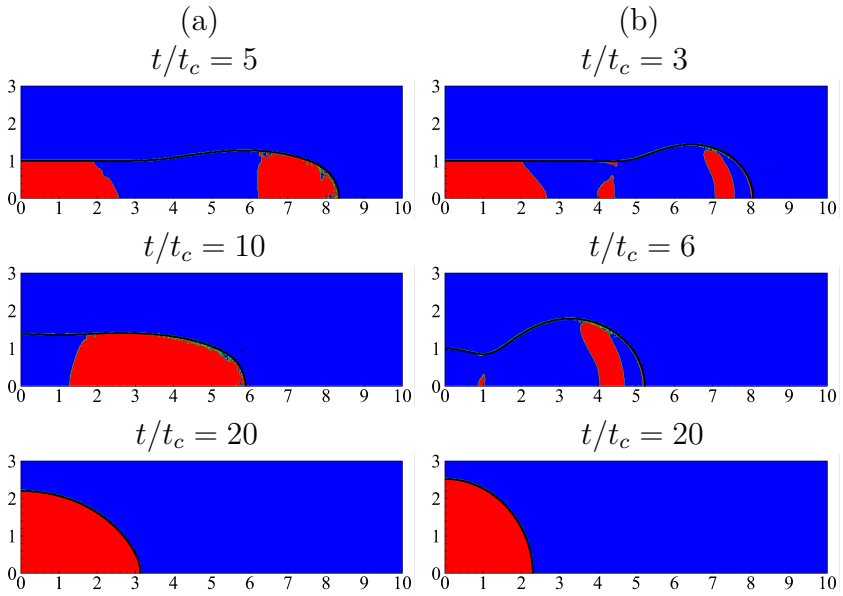


Figure 8. The yielded (blue) and unyielded (red) regions within the viscoplastic slender drops for (a) $Oh = 0.4$, $Pl = 0.9$ and (b) $Oh = 0.1$, $Pl = 0.9$ at different time instants. The interface profile at each time instant is shown by the black line.

$Oh$ value is lower in this case (maximum $Oh \approx 1.15$) for same value of $Oh \times Pl$ as compared with $Pl$ =0.1 or 0.25. The deviations is even more significant for $Pl = 0.9$ (maximum $Oh \approx 0.641$).

Why non-negligible inertia effects, i.e. small Ohnesorge numbers, lead to significant deviation from the theoretical prediction? The first explanation is related to the assumptions used to derive Eq. (11). We assumed that the Ohnesorge number is sufficiently large to neglect the inertial term in the momentum equation. For a lower value of the Ohnesorge number, the inertial term becomes non-negligible and as a result, a significant deviation is observed with the theory. Non-negligible inertia may also lead to the significant deformation of drop/sheet in contrast to our assumption of uniform cylindrical shape. This is evident in Fig. 8 which shows the shape of the

drop at different time instants along with the yielded/unyielded region for $Pl = 0.9$ and two different values of $Oh$. For $Oh = 0.4$ we see a bulbous region close to the tip and the region far away from the tip remains undisturbed (see at $t/t_c = 5$ in Fig. 8 (a)). Finally, the drop retracts to an ellipse like shape. With further increase in inertia, the liquid of the retracting portion of the drop accumulates in the form of a blob at the tip. This is evident in Fig. 8 (b) which shows the simulation results for $Oh = 0.1$ and $Pl = 0.9$.

The inertial contribution causes more retraction than that predicted by the present theory. As a result, the final radius of the drop is higher on such cases than the prediction by Eq. (22). This is evident in Fig. 7 for $Pl = 0.5$ and 0.9. On the other hand, we observe that the final radius of the drop is lower than that predicted by Eq. (22) for $Pl = 0.1$ and 0.25. This is because the length of the drop becomes comparable to its radius towards the later stage of retraction and as a result the slender approximation is no longer valid. This deviation is similar to that discussed in Sec. 3 (see Fig. 5). It is worth noting here that the conservation of mass brings a limitation to the theoretical prediction beyond the point where the drop reaches the spherical shape. In Fig. 7, the green dashed line represents the radius of a spherical drop having the same volume as that of a slender drop of initial aspect ratio $L_0/R_0$ =10, which is the initial aspect ratio in all the numerical simulations considered here. The theoretical prediction of Eq. (22) is irrelevant below the point where the black line intersects this green dashed line ($Oh \times Pl \approx 0.237$) as the drop reaches the spherical equilibrium shape. The retraction is expected to stop when a drop reaches this equilibrium stage. However, if inertia is significant the retraction does not stop even

when the drop reaches a spherical shape; the drop may undergo a prolate-oblate oscillation depending on the value of $Oh$ and the final shape of the drop is quite unpredictable on such a situation [9].

The present model is based on the assumption that the effect of inertia is negligible and that the drop/sheet is slender. The former assumption is always valid at the start of retraction because the yield stress is sufficiently large to resist the appearance of momentum in the blob. The model gives a good prediction for the start of retraction provided that the aspect ratio of the drop is larger than 2.5. The model also gives a good prediction of the final shape of the drop at large $Oh$ (negligible inertia). If the inertia effect becomes important which also leads to significant deformation of the drop, the final shape of the drops/sheets may deviate from that predicted by the present model.

**Acknowledgements**

The authors acknowledge the anonymous referees for their constructive criticism. Hiranya Deka also acknowledges Neil J Balmforth for the valuable discussions and suggestions. Financial support of IFP Energies Nouvelles is gratefully acknowledged.

[1] A. Dupré, Sixiéme memoire sur la theorie méchanique de la chaleu, Ann. Chim. Phys. 4 (11) (1867) 194–220.

[2] G. I. Taylor, The dynamics of thin sheets of fluid. III. Disintegration of fluid sheets, Proceedings of the Royal Society of London. Series A. Mathematical and Physical Sciences 253. doi:10.1098/rspa.1959.0196.

[3] F. E. C. Culick, Comments on a ruptured soap film, Journal of Applied Physics 31 (6) (1960) 1128–1129. doi:10.1063/1.1735765.

[4] W. R. McEntee, K. J. Mysels, Bursting of soap films. I. An experimental study, The Journal of Physical Chemistry 73 (9) (1969) 3018–3028. doi:10.1021/j100843a042.

[5] M. P. Brenner, D. Gueyffier, On the bursting of viscous films, Physics of Fluids 11 (3) (1999) 737–739. doi:10.1063/1.869942.

[6] N. Savva, J. W. M. Bush, Viscous sheet retraction, Journal of Fluid Mechanics 626 (2009) 211–240. doi:10.1017/S0022112009005795.

[7] J.-L. Pierson, J. Magnaudet, E. J. Soares, S. Popinet, Revisiting the Taylor-Culick approximation. Retraction of an axisymmetric filament , Physical Review Fluids (in press).

[8] H. Deka, J.-L. Pierson, Revisiting the Taylor-Culick approximation. Retraction of a viscous sheet , Physical Review Fluids (in revision).

[9] H. Deka, J.-L. Pierson, E. J. Soares, Retraction of a viscoplastic liquid sheet, Journal of Non-Newtonian Fluid Mechanics 272 (2019) 104172. doi:https://doi.org/10.1016/j.jnnfm.2019.104172.

[10] P. P. Mosolov, V. P. Miasnikov, Variational methods in the theory of the fluidity of a viscous-plastic medium, Journal of Applied Mathematics

and Mechanics 29 (3) (1965) 545 – 577. doi:https://doi.org/10.1016/0021-8928(65)90063-8.

[11] P. Mosolov, V. Miashikov, On stagnant flow regions of a viscous-plastic medium in pipes, Journal of Applied Mathematics and Mechanics 30 (4) (1966) 841 – 854. doi:https://doi.org/10.1016/0021-8928(66)90035-9.

[12] A. N. Beris, J. A. Tsamopoulos, R. C. Armstrong, R. A. Brown, Creeping motion of a sphere through a bingham plastic, Journal of Fluid Mechanics 158 (1985) 219–244. doi:10.1017/S0022112085002622.

[13] N. Dubash, I. Frigaard, Conditions for static bubbles in viscoplastic fluids, Physics of Fluids 16 (12) (2004) 4319–4330. doi:10.1063/1.1803391.

[14] J. Tsamopulos, Y. Dimakopoulos, N. Chatzidai, G. Karapetsas, M. Pavlidis, Steady bubble rise and deformation in newtonian and viscoplastic fluids and conditions for bubble entrapment, Journal of Fluid Mechanics 601 (2008) 123–164. doi:10.1017/S0022112008000517.

[15] J. Eggers, Post-breakup solutions of Navier-Stokes and Stokes threads, Physics of Fluids 26 (7) (2014) 072104. doi:10.1063/1.4890203.

[16] N. Balmforth, N. Dubash, A. C. Slim, Extensional dynamics of viscoplastic filaments: I. Long-wave approximation and the Rayleigh instability, Journal of Non-Newtonian Fluid Mechanics 165 (19) (2010) 1139 – 1146. doi:https://doi.org/10.1016/j.jnnfm.2010.05.012.

[17] Basilisk, http://basilisk.fr.

[18] S. Popinet, An accurate adaptive solver for surface-tension-driven interfacial flows, Journal of Computational Physics 228 (16) (2009) 5838 – 5866. doi:https://doi.org/10.1016/j.jcp.2009.04.042.

[19] P.-Y. Lagrée, L. Staron, S. Popinet, The granular column collapse as a continuum: validity of a two-dimensional Navier-Stokes model with a $mu(I)$-rheology, Journal of Fluid Mechanics 686 (2011) 378–408. doi:10.1017/jfm.2011.335.

[20] S. Popinet, A quadtree-adaptive multigrid solver for the Serre-GreenNaghdi equations, Journal of Computational Physics 302 (2015) 336 – 358. doi:https://doi.org/10.1016/j.jcp.2015.09.009.

[21] E. C. Bingham, Fluidity and Plasticity, McGraw-Hill Book Company, New York, 1922.

[22] R. L. Thompson, E. J. Soares, Viscoplastic dimensionless numbers, Journal of Non-Newtonian Fluid Mechanics 238 (2016) 57 – 64. doi:https://doi.org/10.1016/j.jnnfm.2016.05.001.

[23] J. Eggers, T. F. Dupont, Drop formation in a one-dimensional approximation of the navierstokes equation, Journal of Fluid Mechanics 262 (1994) 205221. doi:10.1017/S0022112094000480.

[24] G. German, V. Bertola, Formation of viscoplastic drops by capillary breakup, Physics of Fluids 22 (3) (2010) 033101. doi:10.1063/1.3339783.

[25] G. German, V. Bertola, The spreading behaviour of capillary driven yield-stress drops, Colloids and Surfaces A Physicochemical and Engineering Aspects 366 (2010) 18–26. doi:10.1016/j.colsurfa.2010.05.019.

[26] T. Erneux, S. H. Davis, Nonlinear rupture of free films, Physics of Fluids A: Fluid Dynamics 5 (5) (1993) 1117–1122. doi:10.1063/1.858597.

[27] I. Frigaard, C. Nouar, On the usage of viscosity regularisation methods for visco-plastic fluid flow computation, Journal of Non-Newtonian Fluid Mechanics 127 (1) (2005) 1 – 26. doi:https://doi.org/10.1016/j.jnnfm.2005.01.003.